Self-Assembling of Phenothiazine Compounds Investigated by Small-Angle X-ray Scattering and Electron Paramagnetic Resonance Spectroscopy

Leandro R. S. Barbosa and Rosangela Itri*

Instituto de Física da Universidade de São Paulo, Cx. Postal 66318, CEP 05315-970 − São Paulo, SP, Brazil

Wilker Caetano

DFQB, Faculdade de Ciências e Tecnologia, UNESP, CEP 19060-900, Presidente Prudente, SP, Brazil

Diógenes de Sousa Neto and Marcel Tabak

Instituto de Química de São Carlos, Universidade de São Paulo, Cx. Postal 780, CEP 13560-970 − São Carlos, SP, Brazil

Received: October 25, 2007; In Final Form: January 18, 2008

Small-angle X-ray scattering (SAXS) and electron paramagnetic resonance (EPR) have been carried out to investigate the structure of the self-aggregates of two phenothiazine drugs, chlorpromazine (CPZ) and trifluoperazine (TFP), in aqueous solution. In the SAXS studies, drug solutions of 20 and 60 mM, at pH 4.0 and 7.0, were investigated and the best data fittings were achieved assuming several different particle form factors with a homogeneous electron density distribution in respect to the water environment. Because of the limitation of scattering intensity in the q range above 0.15 $Å^{-1}$, precise determination of the aggregate shape was not possible and all of the tested models for ellipsoids, cylinders, or parallelepipeds fitted the experimental data equally well. The SAXS data allows inferring, however, that CPZ molecules might self-assemble in a basis set of an orthorhombic cell, remaining as nanocrystallites in solution. Such nanocrystals are composed of a small number of unit cells (up to 10, in c-direction), with CPZ aggregation numbers of 60−80. EPR spectra of 5- and 16-doxyl stearic acids bound to the aggregates were analyzed through simulation, and the dynamic and magnetic parameters were obtained. The phenothiazine concentration in EPR experiments was in the range of 5−60 mM. Critical aggregation concentration of TFP is lower than that for CPZ, consistent with a higher hydrophobicity of TFP. At acidic pH 4.0 a significant residual motion of the nitroxide relative to the aggregate is observed, and the EPR spectra and corresponding parameters are similar to those reported for aqueous surfactant micelles. However, at pH 6.5 a significant motional restriction is observed, and the nitroxide rotational correlation times correlate very well with those estimated for the whole aggregated particle from SAXS data. This implies that the aggregate is densely packed at this pH and that the nitroxide is tightly bound to it producing a strongly immobilized EPR spectrum. Besides that, at pH 6.5 the differences in motional restriction observed between 5- and 16-DSA are small, which is different from that observed for aqueous surfactant micelles.

1. Introduction

Chlorpromazine (CPZ) and trifluoperazine (TFP) (Figure 1) are two important phenothiazine compounds that have a great variety of biological, medical, and chemical properties, being commonly used in clinics as antidepressant and antipsychotic drugs.[1−4] Under physiological conditions they are amphiphilic cationic compounds, which consist of a hydrophobic nitrogen-containing heterocycle bound to a short chain containing a charged amino group. The study of the phenothiazine aggregates has gained much attention because of their photosensitizing effects in patients under therapy.[5,6] Extracorporeal photochemotherapy has also been used with phenothiazines for the treatment of a number of diseases.[7−9] Furthermore, this kind of compound has interesting physicochemical behavior associated with their capacity to change the properties of natural and model biomembranes.[10−15]

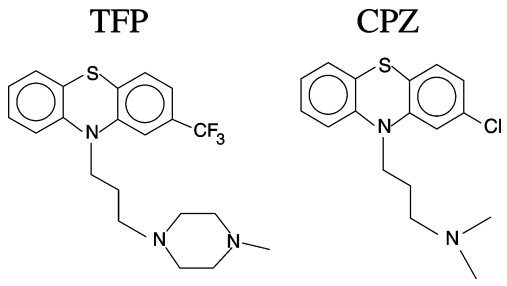

Figure 1. Chemical structures of phenothiazine compounds, chlorpromazine (CPZ) and trifluoperazine (TFP), used in this work.

Recent structural studies by means of small-angle X-ray scattering (SAXS) have been concerned with comicellization properties of CPZ and TFP with zwitterionic HPS (3-(*N*-hexadecyl-*N*,*N*-dimethylammonium)propanesulfonate)[11] and LPC

* Author for correspondence. E-mail: itri@if.usp.br; fax: 55-11-3091-6749.

10.1021/jp710332t CCC: $40.75
Published on Web 03/18/2008

(L-α-lysophosphatidylcholine)[12] as well as anionic SDS (sodium dodecyl sulfate) micelles.[10] SAXS results reveal changes in the shape and size of the drug/surfactant comicelles, which were dependent on the surfactant surface-charge, the type and protonation state of the drug, the surfactant concentration, and the surfactant:phenothiazine molar ratio. Noteworthy, TFP and CPZ can have distinct physical−chemical properties, because of the difference in the protonation state of each molecule (see the number of amino groups in Figure 1).

Concerning the phenothiazine self-aggregation properties, a recent study has explored the photochemical behavior of three phenothiazine derivatives in aqueous solution (thioridazine, TR; fluphenazine, TF; trifluoperazine, TFP) in the monomeric and aggregated form,[16] through several techniques, such as EPR (electron paramagnetic resonance), SAXS, electronic absorption, among others. The combined results gave support to conclude that, although the phenothiazines self-assembled at concentrations above 100 μM, only TR formed large lamellar-like structures at 25 mM, pH 4.0.[16] Interestingly, such arrangement resembles that observed in its native crystallographic cell.[17] Small-angle neutron scattering (SANS) has been previously employed to investigate the structural properties of aqueous (D_2O) solutions of pure CPZ.[18] The data were characteristic of systems with strong correlations, mainly due to electrostatic interactions between charged aggregates. Furthermore, evidence from NMR studies[19−22] of the chemical shift changes of aromatic protons and carbon atoms of CPZ over a wide range of solution concentration has provided information on the spatial arrangements of the two molecules forming a dimer, where a concave-to-convex vertical stacking of the aggregate with the alkyl side chains on alternate sides of the stack has been proposed.[19−22]

Despite a considerable amount of research dealing with the effects of phenothiazines in self-assembling or even in the comicellization with mimetic membranes, their mechanism of action remains not well understood at the molecular level. In order to further elucidate the structural features of phenothiazine aggregates, in the current work we extend our previous studies on TFP and CPZ,[10−12] making use of the SAXS technique. The measurements were conducted at high drug concentrations, in the milimolar range, because of the sensitivity of the technique, and the scattering data were analyzed through the modeling of the homogeneous particle form factor and the interparticle interference function. In order to obtain additional information on the molecular dynamics of the phenothiazine aggregates, electron paramagnetic resonance (EPR) experiments, with the use of nitroxide spin labels, were performed for samples similar to those used in the SAXS studies.

2. Materials and Methods

2.1. Experimental. Chlorpromazine hydrochloride (CPZ) and trifluoperazine dihydrochloride (TFP, Sigma Chem. Co.), sodium acetate, and monobasic sodium phosphate (Mallinckrodt) were used as purchased. In general, 20 mM of buffer (sodium acetate or phosphate, respectively, at pH 4.0 or 7.0) in ultrapure Milli-Q (18.2 MΩ.cm) water has been employed. The pH values were adjusted with calibrated solutions of HCl and NaOH and measured using either a Corning-130 or a Digimed pH meters. Phenothiazine micellar solutions of 20 and 60 mM, in the appropriate buffer, were prepared in eppendorf test tubes at each chosen pH (initial measurements with glass test tubes showed that the phenothiazines adhere to the tubes). The drug concentrations in the samples were checked after the experiment by dilution and measurement of the electronic absorption spectra at the appropriate wavelenghts.[23,24] The mixture was equilibrated for at least 48 h prior to the experiments.

SAXS experiments were performed at National Laboratory of Synchrotron Light (LNLS, Campinas, Brazil) at room temperature of 22 ± 1 °C, with radiation wavelength $\lambda = 1.608$ Å and sample-to-detector distance of ∼600 mm. Samples were conditioned in sealed 1 mm thick acrylic cells, with mylar windows, perpendicular to the incident X-ray beam. The obtained curves (data collection of 15 min) were corrected for detector inhomogeneity (one-dimension position-sensitive detector) and normalized by taking into account the decrease of the X-ray beam intensity during the experiment. The parasitic background (buffer solution) was subtracted, considering the sample's attenuation. Two sets of measurements were taken from each sample after a time interval of 2−4 h, showing reproducible scattering data. The final spectra correspond to an average of the corrected data for each studied sample.

Samples for EPR experiments were prepared in the following way: small microliter aliquots of stock 10 mM ethanol solutions of nitroxide spin probes 5- and 16-doxyl stearic acids (Aldrich, used as received) were added to eppendorf test tubes. After the solvent was dried, the previously prepared phenothiazine solutions at a fixed concentration in the range 5−60 mM, and in appropriate buffer as described above, were added in such a way that the final nitroxide concentration was 10^{-4} M.

2.2. Methods. *2.2.1. SAXS Data Analysis.* The SAXS intensity $I(q)$ of an isotropic solution of monodisperse particles of low anisometry ν (ratio between the longest and the shortest axes smaller than 3) is described by[25,26]

$$I(q) = k\,P(q)\,S(q) \tag{1}$$

where k is a normalization factor that depends on the particle number density and on the instrumental effects ($q = (4\pi/\lambda)\sin\theta$ is the scattering vector, 2θ being the scattering angle).

$P(q)$ (eq 1) represents the orientational average of the scattering particle form factor, and in the absence of interference effects ($S(q) \approx 1$) it can be connected through a Fourier transform to the pair distance distribution function, $p(r)$, which is associated with the probability of finding a small pair of elements at a distance r within the entire volume of the scattering particle. Under such conditions, these functions can be written as[25,27]

$$p(r) = \left(\frac{1}{2\pi^2}\right)\int_0^\infty I(q)qr\,\sin(qr)\mathrm{d}q \tag{2}$$

and

$$I(q) = 4\pi\int_0^{D_{\max}} p(r)\,\frac{\sin(qr)}{qr}\,\mathrm{d}r \tag{3}$$

The $p(r)$ function can provide information about the shape and the maximum dimension ($D_{\max}$) of the scattering particle. In the present work, we made use of the *GIFT* software, developed by O. Glatter,[27] to obtain the $p(r)$ function. Moreover, the particle radius of gyration (R_g) is obtained from $p(r)$ through[27−29]

$$R_g^{\,2} = \frac{\int_0^{D_{\max}} p(r)r^2dr}{2\int_0^{D_{\max}} p(r)\mathrm{d}r} \tag{4}$$

In terms of the $P(q)$ function, regarding the particle morphology, three different aggregate geometries were tested in the current work. They were prolate ellipsoidal-like, cylinder-like, and parallelepiped-like shapes. In fact, as it will be shown later

in the text, the $P(q)$ modeling of these geometries is quite similar over the experimental scattering curve for small ν values. In this way, it will not be possible here to infer about the precise aggregate shape but only about its dimension. Concerning the ellipsoidal and the cylindrical form factors, the $P(q)$ functions are described elsewhere,[25,27,28] having the shortest axis (R) and the anisometry ν as free parameters (total length $H = 2\nu R$). The $P(q)$ function for a parallelepiped-like scattering particle in solution, with edges A, B, and C, is given by:[28]

$$P(q) = \frac{2}{\pi}\left\{\int_0^1 \mathrm{Y}^2\left(\frac{qCx}{2}\right)\int_0^{\pi/2} \mathrm{Y}^2(0.5qA\sin(y))\mathrm{Y}^2(0.5qB(1-x^2)^{1/2}\cos(y))\mathrm{d}y\mathrm{d}x\right\} \quad (5)$$

where $\mathrm{Y}(t) = \sin(t)/t$

Moreover, concerning another work dealing with phenothiazine aggregates, Perez-Villar et al.[18] studied the CPZ aggregate behavior, by means of SANS (small angle neutron scattering) technique. The authors modeled the scattering functions by using a core−shell scattering length contrast, typical of micelle-like aggregates. However, we have noticed that, because of the dimension of the scattering particle, the existence of an internal structure of the phenothiazine aggregate could be assessed only for q values larger than 0.3 Å^{-1}, outside our experimental q range.

$S(q)$ in eq 1 corresponds to the interparticle interference function. In this work, we made use of Hayter and Penfold's methodology,[30,31] which associates the scattering particle as a charged sphere (with equal volume of the scattering particle), interacting through a screened Coulomb potential, in a mean spherical approximation (MSA). This approximation, however, is only valid for particles of small values of ν (smaller than 3).[26] In this way, the surface potential of an "equivalent sphere" is related to another free parameter, the ionization coefficient α, which could be interpreted as the effective charge in the scattering particle surface ($\alpha = z/n$, where z and n are the total surface charge and the aggregation number, respectively). It should be stressed that α has to be considered as an "effective value", since as a free parameter it can suppress the deficiencies of the potential accounted for in this methodology.[32] The structural parameters and α are then obtained by fitting the product $P(q) \times S(q)$ to the experimental curve.

EPR Data Analysis. EPR spectra were run on a Varian E-9 spectrometer at room temperature using the following parameters: microwave frequency, 9.515 GHz; microwave power, 20 mW; center magnetic field, 340.5 mT; sweep width, 10 mT; sweep time, 2 min; modulation frequency, 100 kHz; modulation amplitude, 0.1 mT; detector time constant, 0.064 s. Samples were accommodated in microcapillary tubes sealed on both sides and adjusted inside a 3 mm EPR quartz tube. Semiquantitative estimates of molecular mobility by EPR based on a previous approach described for small molecule−membrane interaction studies[33−35] and using the intensities of the three-component EPR spectra and line width of the central line[36,37] were not possible because of the significant immobilization of radical motion precluding the use of this calculation. For this reason EPR spectra were simulated using the nonlinear least-squares (NLLS) simulation program developed by Freed's group,[38] using the general slow-motional program.[38,39] The magnetic g and A tensors are defined in a molecule-fixed frame, where the rotational diffusion rates around the x-, y-, and z-axis are included.[38,39] By convention, the x-axis points along the N−O bond, the z-axis is parallel to the 2pz axis of the nitrogen atom, and the y-axis is perpendicular to x and z.[36,38,39] The fitting program NLLS permits to estimate the rotational motion around the axes x, y, and z (the diffusion tensor $\mathbf{R}$) for a single or multicomponent EPR spectra. However, in order to reduce the number of free parameters and to simplify the simulation, we assume in some cases, as described in ref 40, an axially symmetric rotational diffusion tensor with $\mathbf{R}_{bar} = (\mathbf{R}_\perp^2\ \mathbf{R}_\parallel)^{1/3}$ and a rotational anisotropy with $\mathbf{R}_\parallel = 10\mathbf{R}_\perp$[39]. The magnetic parameters g and A tensors, as well as the additional line widths, were optimized for all the spectra simulated in this paper. In some special cases, for some experimental conditions, the simulation of EPR spectra was not possible because of the presence of spin−spin interaction. An alternative calculation was made of an effective order parameter, S, which describes the orientational distribution of the nitroxides relative to the normal of the aggregates (micelles, phospholipid bilayers, etc.). This calculation was performed as described in refs 36 and 41.

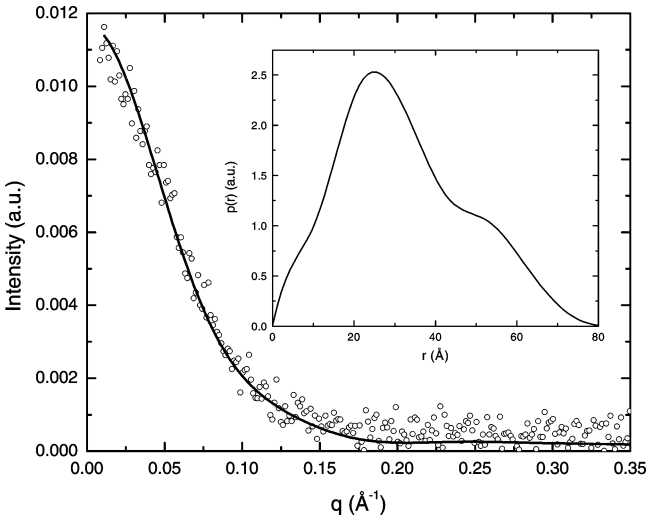

Figure 2. SAXS curve from the system composed of 20 mM CPZ in aqueous solution at pH 7.0. The solid line represents the theoretical $I(q)$ function (eq 3) along with the experimental data (open symbols). The corresponding pair distance distribution function $p(r)$ (eq 2) is presented in the insert.

3. Results and Discussion

3.1. SAXS Data. Aqueous solutions of 20 mM CPZ, at pH 4.0, did not produce a detectable SAXS signal, whereas at pH 7.0 a significant scattering takes place (Figure 2), without any influence of interaggregates interaction. This behavior must be due to the difference of the protonation state at these pH values. In a more acidic environment, there are more CPZ molecules in the protonated form, as compared to the neutral form, providing a higher electrostatic repulsion between the aliphatic tails, inhibiting the CPZ aggregation. From the $p(r)$ analysis, displayed in Figure 2, the maximum particle dimension and radius of gyration of $D_{max} = 80$ Å and $R_g = 25$ Å, respectively, were obtained. The latter is in good agreement with the value obtained by the Guinier's law.[25] The $p(r)$ function resembles that found for randomly distributed homogeneous anisometric particles.[27] From the ratio between the $p(r)$ inflection point (∼35 Å) and D_{max}, one can roughly estimate the anisometry ν (≈2.3) of the CPZ aggregate.[27,28]

Moreover, by taking into account the obtained values of R_g and D_{max}, one can evaluate the particle cross-section dimension for simple anisometric particles such as prolate ellipsoids or cylinders as 40 Å and 32 Å, respectively. These two values are on the same order of magnitude as that roughly evaluated from the $p(r)$ analysis (inflection point of *ca.* 35 Å). So, it was not

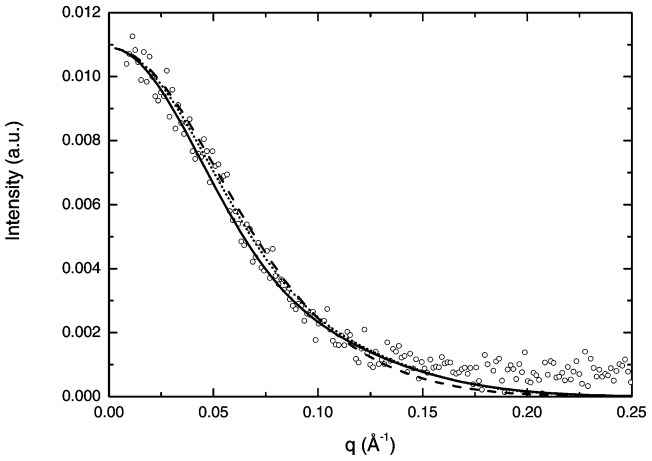

Figure 3. Form factor $P(q)$ simulations from the system composed of CPZ (20 mM) at pH 7.0 (open circles). The solid, short-dotted, and dashed lines correspond to the parallelepiped (with edges equal to 25 Å, 25 Å, 80 Å), the cylinder (with R and ν equal to 15 Å and 2.4, respectively), and the prolate ellipsoid (with R and ν equal to 18 Å and 2.4, respectively) $P(q)$ functions.

possible to distinguish, by using this criterion, between the cylinder and the ellipsoid models for the shape of the aggregate. However, the information extracted from $p(r)$ analysis in terms of the anisometric form and cross-section dimension for the CPZ aggregates is consistent with the spatial arrangement previously proposed from NMR studies,[19−22] which consists of an off-set concave-to-convex vertical stacking of the CPZ molecules with the alkyl side chains on alternate sides of the stack.

Furthermore, an orthorhombic crystallographic structure for CPZ crystals with a basis set of $a = 23.5$ Å, $b = 15.2$ Å, and $c = 9.2$ Å, has been previously proposed by McDowell.[17] The unit cell is composed by eight CPZ molecules with four molecules "left-handed" (type 1) and four "right-handed" (type 2) in an enantiomorph configuration. The two sets of CPZ molecules, types 1 and 2, were linked by chloride atoms. In another work, Klein and Conrad III[42] observed a monoclinic arrangement of CPZ with $a = 11.9$ Å, $b = 31.7$ Å, $c = 9.6$ Å, and an angle of approximately 99°. Both reports[17,42] agree regarding the cell volume and the number of CPZ molecules in the unit cell, namely 8.

In order to better explore the possibility of CPZ molecules in solution to self-assemble as a precursor to its further crystalline arrangement, the form factor of a parallelepiped-like aggregate (eq 5) has also been considered as that corresponding to the anisometric scattering particle. In this context, Figure 3 shows the $P(q)$ functions for cylinder-like, parallelepiped-like and ellipsoidal-like CPZ aggregates with $R_g = 25$ Å and $D_{max} = 80 \pm 10$ Å. All of them provide a good fit to the experimental scattering curve of 20 mM CPZ in aqueous solution at pH 7.0.

As one can see from Figure 3, it is not precisely possible to infer about the morphology of CPZ aggregates, but only about their dimension, since all anisometric form factors used for the fits resulted in rather good agreement with the experimental data. Actually, by means of the SAXS technique, it is not possible to distinguish between small cylinders, ellipsoids, or parallelepipeds because the rotational averages of these particles in solution lead to very similar $P(q)$ functions.[27,28]

So, in order to get information on the values of radius R and anisometry ν (corresponding to the total aggregate length H, Table 1), that allows us to estimate the aggregation number N, we decided to proceed with data analysis by using a cylindrical shape for $P(q)$ in eq 1. Ellipsoids and parallelepipeds with cylinder equivalent volumes would lead to similar results within the experimental q region. In this way, an aggregation number N of 154 CPZ molecules is obtained from the cylinder volume V calculation (Table 1), when a CPZ molecular volume of 254 Å^3 is considered from molecular energy optimization (Gaussian software package). However, such an estimate presumes that the whole particle volume is completely filled by CPZ molecules and does not take into consideration either the molecule geometry or the thermodynamic stability of the molecular stacking. According to the off-set concave-to-convex stacking model previously proposed by NMR studies,[19−22] such an aggregation number, N, should be indeed divided by 2, which would lead to a value of ≈77 molecules for the CPZ aggregate at 20 mM in aqueous solution.

Focusing on the parallelepiped-like aggregate possibility, Figure 4a shows the $P(q)$ function based on MacDowell work,[17] with parallelepiped edges equal to 23.5 Å, 15.5 Å, and 80(or 90) Å, corresponding to the basis set of an orthorhombic system with 8 to 10 unit cells stacked in c-direction, i.e., vertical stacking. Moreover, on the basis of Klein and Conrad III,[42] SAXS intensity simulation was carried out (Figure 4b) showing a good agreement with the experimental data for a parallelepiped of edges 31.7 Å, 12.0 Å, and 80 Å. Interestingly, the total unit cell number also amounts to 8−10. Therefore, if a number of 8 CPZ molecules for the unit cell is taken into account, as proposed for the crystalline structure,[17,42] an aggregation number of 64−80 CPZ molecules is found, in good agreement with the volume analysis presented above.

Taking together, the combined results of SAXS and theoretical $P(q)$ simulations might shed light and provide interesting

TABLE 1: Values of the Adjustment Parameters Obtained from the Scattering Curves of Samples Composed of 20 and 60 mM TFP and CPZ at pH 4.0 and 7.0, through $P(q)$ for a Cylinder-like Model and $S(q)$ Function (eq 1)

drug	[drug]	R^a (Å)	ν^b	α^c	H^d (Å)	V^e (Å^3)	$N/2^f$	τ^g (ns)
				pH 7.0				
TFP	20 mM	12.5 ± 0.5	2.5 ± 0.3	0.10 ± 0.01	62 ± 8	(3.1 ± 0.4) × 10^4	59 ± 8	10 ± 1
	60 mM	11.2 ± 0.3	1.8 ± 0.1	0.07 ± 0.01	40 ± 2	(1.6 ± 0.1) × 10^4	30 ± 2	5.0 ± 0.3
CPZ	20 mM	12.5 ± 0.8	3.2 ± 0.3	no interf	80 ± 9	(3.9 ± 0.5) × 10^4	77 ± 10	12 ± 2
	60 mM	14.2 ± 0.6	1.7 ± 0.1	0.05 ± 0.01	48 ± 3	(3.0 ± 0.2) × 10^4	59 ± 4	10 ± 1
				pH 4.0				
TFP	20 mM	10 ± 1	2.3 ± 0.3	0.12 ± 0.01	46 ± 8	(1.4 ± 0.2) × 10^4	26 ± 4	5 ± 1
	60 mM	9.1 ± 0.5	2.4 ± 0.3	0.14 ± 0.01	44 ± 6	(1.1 ± 0.2) × 10^4	22 ± 4	4 ± 1
CPZ	20 mM	no aggreg						
	60 mM	9.3 ± 0.5	3.0 ± 0.3	0.22 ± 0.01	56 ± 6	(1.6 ± 0.2) × 10^4	31 ± 4	5 ± 1

[a] $2R$ = Cross-section diameter. [b] ν = Axial ratio between the longest and the shortest paraffinic axes. [c] α = Ionization coefficient. [d] $H = 2\nu R$. [e] $V = \pi R^2 H$. [f] $N = V/\text{vol}$, where vol = 254 and 264 Å^3 for CPZ and TFP molecules, respectively. [g] Rotational correlation times for the phenothiazine aggregates as a whole particle, estimated from Debye−Stokes relation $\tau = \eta V/RT$, where η is the solution viscosity, V is the particle volume, T is the temperature, and R is the gas constant.

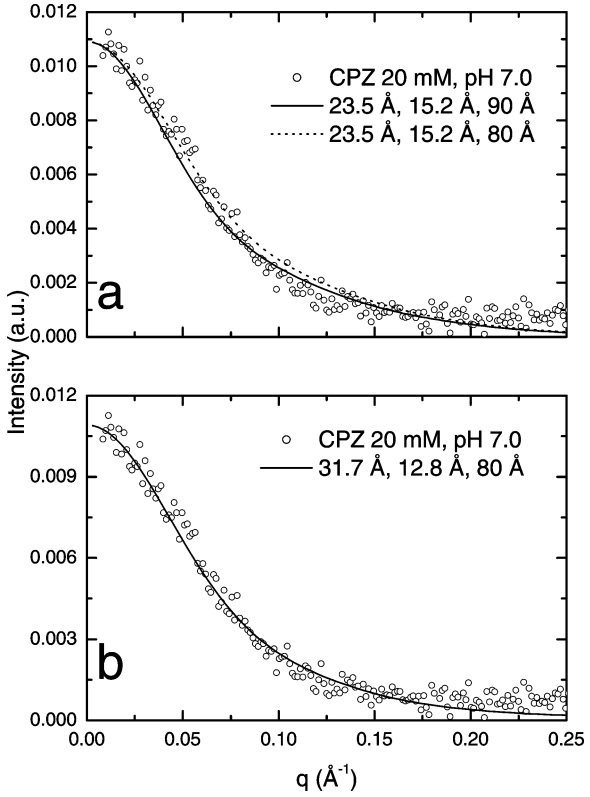

Figure 4. Form factor simulations of parallelepipeds based on the CPZ crystallographic structure proposed by (a) MacDoweel[17] and (b) Klein and Conrad III[42] (see text for details).

information concerning CPZ aggregates. Such phenothiazine molecules in the process of assembling might self-aggregate as those in the unit cell of the crystalline structure, remaining as nanocrystallites in solution composed of a small number of unit cells (up to 10, in *c*-direction).

Regarding CPZ at higher concentrations and TFP solutions, all SAXS curves present interference functions as described below. Again, as it is not possible to be sure about the precise aggregate shape, as discussed above, a cylindrical model for $P(q)$ was used in eq 1 to obtain information on parameters R and H that characterize the aggregate dimensions.

Figure 5 shows the SAXS curves for the systems composed of 20 mM TFP at pH 4.0 (open circles) and 7.0 (open squares) along with the best fits. Table 1 contains the fitting parameters. The corresponding form factors $P(q)$ and the interference functions $S(q)$ are displayed in the insert. As one can see, there were no significant differences in the $S(q)$ functions. Such a behavior was not initially expected, since at pH 4.0 TFP should be partially diprotonated whereas at pH 7.0 only partially monoprotonated. This would lead to a stronger repulsion between TFP aggregates at pH 4.0. On the other hand, the aggregates are smaller at pH 4.0 as compared to pH 7.0 as revealed by the values of total length and aggregation number (Table 1). There is a shrinkage in the cross-section radius from 12.5 ± 0.5 Å at pH 7.0 to 10 ± 1 Å at pH 4.0 (Table 1). Maybe a stronger interaction between TFP molecules at pH 4.0 indeed takes place, which would lead to the formation of smaller aggregates than at pH 7.0. Therefore, the results give support to conclude that, at 20 mM, the TFP molecules have a higher hydrophobic interaction than CPZ, since there was no evidence of CPZ aggregation at pH 4.0. As the CPZ molecule can only be monoprotonated, whereas the TFP molecules can be diprotonated, a higher electrostatic repulsion is expected among the

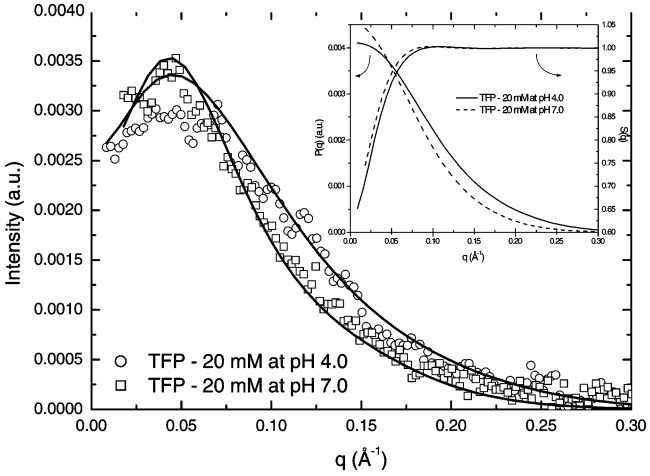

Figure 5. SAXS curves of the systems composed of TFP with 20 mM at pHs 4.0 (open circles) and 7.0 (open squares). The solid lines represent the best fitting obtained through eq 1, adopting the cylindrical form factor. The best fitting parameters are described in Table 1. The insert displays the form factor, $P(q)$, and the interference function, $S(q)$, of each scattering curve.

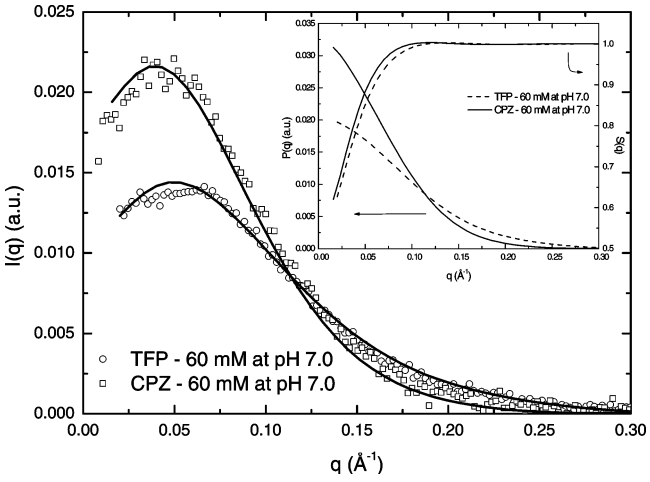

Figure 6. SAXS curves for the systems composed of 60 mM of TFP (open circles) and CPZ (open squares) at pH 7.0. The solid lines represent the best fitting obtained through eq 1, adopting the cylindrical form factor. The best fitting parameters are described in Table 1. The insert displays the form factor, $P(q)$, and the interference function, $S(q)$, of each scattering curve.

TFP molecules in comparison to CPZ. Then, only a stronger hydrophobic contribution could stabilize the TFP aggregates.

The SAXS curves obtained for the samples at higher drug concentrations (60 mM), at pHs 7.0 (Figure 6) and 4.0 (Figure 7), also present broad peaks attributed to the presence of the interparticle interference functions due to the interaction of positively charged phenothiazine aggregates. At pH 7.0 (Figure 6) the data analyses indicate that the molecules self-assemble into smaller aggregates at 60 mM than at 20 mM (Table 1), i.e., the drug molecules prefer to self-associate in a greater number of smaller aggregates at 60 mM as compared to 20 mM. In terms of CPZ and TFP aggregates at 60 mM, they interact quite similarly as revealed by the values of α in Table 1. Nevertheless, CPZ aggregates are wider than the TFP aggregates (Table 1). One possible explanation lies in the hydrophobic effect; since the TFP molecule has major hydrophobic characteristics, the aggregates should be more compact, reflecting a smaller cross-section dimension. Such a reduction reflects on the aggregate volume that is smaller for TFP than CPZ, being also responsible for the depression of $P(q \rightarrow 0)$ for TFP in

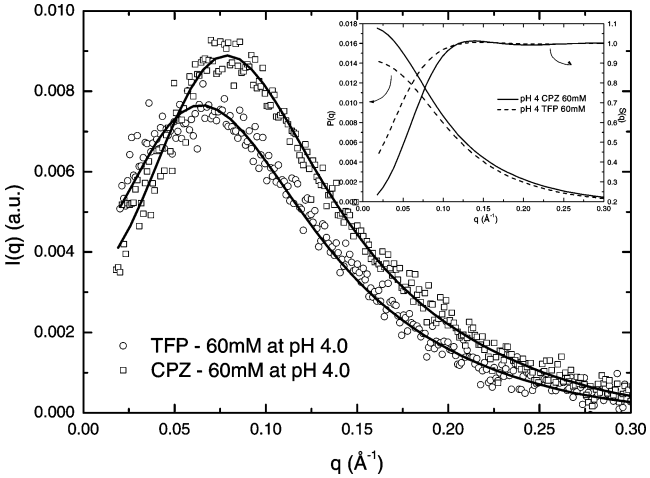

Figure 7. SAXS curves for the systems composed of 60 mM of TFP (open circles) and CPZ (open squares) at pH 4.0. The solid lines represent the best fitting obtained through eq 1, adopting the cylindrical form factor. The best fitting parameters are described in Table 1. The insert displays the form factor, $P(q)$, and the interference function, $S(q)$, of each scattering curve.

comparison to CPZ (insert of Figure 6). By making a parallel with parallelepiped shape and the corresponding crystal arrangement,[17,42] one can suggest that the aggregate might be composed of 4 to 5 unit cells, comprising *ca.* 40 phenothiazine molecules in each aggregate, if a *H* value of 40 to 50 Å (Table 1) is taken into account. Such a number of molecules is consistent with those reported in previous studies using several different techniques.[43−46] In a study by Tehrani et al.,[43] the authors used the quenching of intrinsic fluorescence of CPZ in the aggregates to estimate the aggregation number as a function of phenothiazine concentration and temperature. They showed that at 10 mM CPZ in 0.1 M phosphate buffer (pH 6.5), at 25 °C, the mean aggregation number was 37 ± 5. Because of limitations of the fluorescence technique, aggregation numbers were estimated in a narrow phenothiazine concentration range between 7 and 13 mM and varied from 15 to 55 in this range. In the temperature range between 20 and 35 °C, the mean aggregation number was constant, decreasing below 20 °C and above 40 °C[43]. The estimated value of 37 was in excellent agreement with values obtained from gel filtration chromatography,[44] light scattering,[45] or sedimentation equilibrium,[46] all of them in the range 35−38 and estimated in the presence of 100−150 mM of NaCl. It should be mentioned that in the gel filtration study,[44] strong evidence was obtained for the presence of a dimer of CPZ at low concentration, and a model was used for a stepwise aggregate formation corresponding to a particle of 38 monomers. An important drawback in this study is the fact that the pH was not controlled and increase of CPZ concentration in pure aqueous solution is always accompanied by acidification of the medium which significantly influences the aggregation process, as shown in an early spectroscopic study.[47] In the sedimentation equilibrium study,[46] evidence was obtained for the equilibrium in solution of CPZ monomers with aggregates containing 35 monomers.

At pH 4.0, Figure 7 shows the SAXS curves for the systems composed of 60 mM CPZ and TFP. The behavior of interaggregate interference functions demonstrates that the aggregate surface charge increases at lower pH, probably because of a more effective drug protonation. Moreover, this increase in the surface charge seems to be greater in the CPZ aggregates as compared to TFP aggregates (Table 1). Concurrently, there is a further reduction of cross-section radius in respect to the

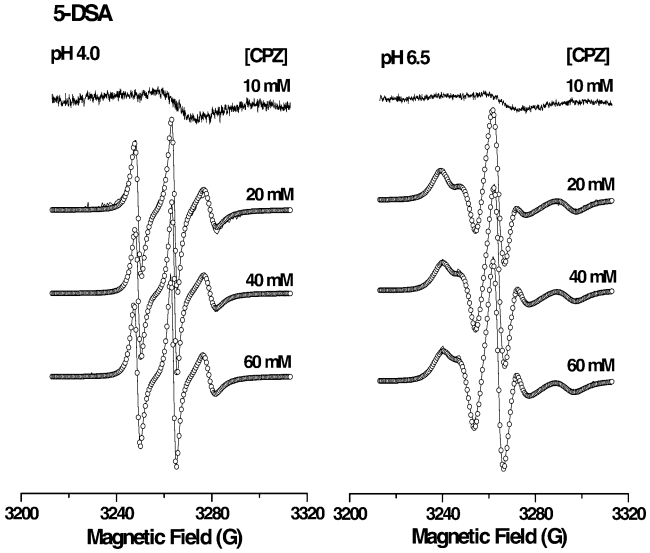

Figure 8. Experimental (full line) and simulated (circles) EPR spectra for 5-DSA bound to CPZ aggregates at indicated drug concentrations and pHs.

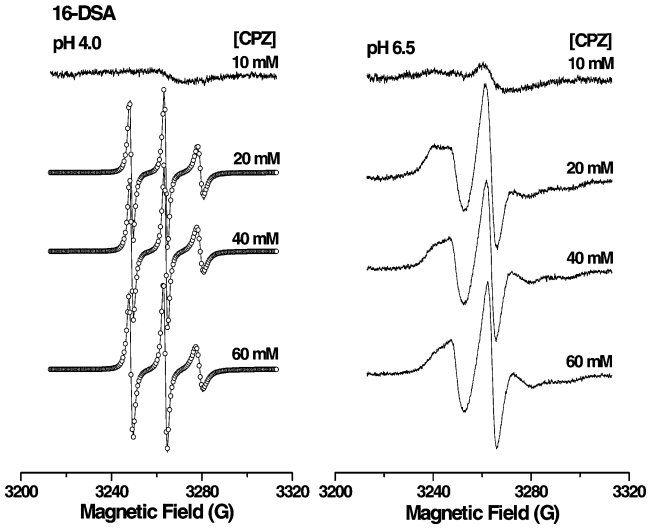

Figure 9. Experimental (full line) and simulated (circles) EPR spectra for 16-DSA bound to CPZ aggregates at indicated drug concentrations and pHs.

aggregates at pH 7.0 (Table 1), and CPZ aggregates are longer than TFP aggregates.

3.2. EPR Data. At this point it is worth commenting on the results obtained from EPR experiments with 5-DSA and 16-DSA for the phenothiazine aggregates described previously in SAXS results. As mentioned in Methods, for EPR experiments, samples of phenothiazines at concentrations in the range 5−60 mM were prepared. In Figures 8 and 9 the experimental EPR spectra for CPZ at two investigated pHs are shown for the two nitroxides. For CPZ concentrations of 5 (not shown) and 10 mM, broadened spectra of low intensity were obtained, which correspond to a relatively small concentration of "micelle-like" phenothiazine-aggregated particles and a strong spin−spin interaction of the nitroxides in these aggregates. This CPZ concentration is consistent with the reported values of critical micellar concentrations (cmc) for this compound. This parameter, which is well defined for aqueous surfactant micelles, has been continuously used in the literature, especially in spectroscopic studies, referring to phenothiazine aggregates. We will keep its use in this paper, even though critical aggregate concentration (CAC) would also be an appropriate term to

TABLE 2: Diffusion Tensor, $\mathbf{R}_{bar}$, Rotational Correlation Times, τ, Hyperfine Tensor Components, A_{ii}, and Isotropic Hyperfine Splitting, a_0, Obtained from Simulation of EPR Spectra (25 °C) of 5-DSA and 16-DSA Incorporated in CPZ Aggregates at Indicated Concentrations, at pHs 4.0 and 6.5

[CPZ]	$\mathbf{R}_{bar}$	τ (ns)	A_{xx} (1)	A_{yy} (1)	A_{zz} (1)	a_0 (1)
			5-DSA/pH 4.0			
20	8.31	0.81	7.19	5.60	33.38	15.39
40	8.31	0.81	7.15	5.56	33.38	15.36
60	8.31	0.81	7.15	5.62	33.26	15.34
			5-DSA/pH 6.5			
20	7.61	4.11	6.81	5.33	33.42	15.19
40	7.68	3.46	7.09	5.52	33.64	15.42
60	7.73	3.13	7.07	5.62	33.73	15.47
			16-DSA/pH 4.0			
20	8.67	0.35	7.14	5.64	33.27	15.35
40	8.59	0.43	7.14	5.64	32.97	15.25
60	8.53	0.49	7.14	5.64	32.89	15.22

TABLE 3: Diffusion Tensor, $\mathbf{R}_{bar}$, Rotational Correlation Times, τ, Hyperfine Tensor Components, A_{ii}, and Isotropic Hyperfine Splitting, a_0, Obtained from Simulation of EPR Spectra (25 °C) of 5-DSA and 16-DSA Incorporated in TFP Aggregates at Indicated Concentrations, at pHs 4.0 and 6.5

[TFP]	$\mathbf{R}_{bar}$	τ (ns)	A_{xx} (1)	A_{yy} (1)	A_{zz} (1)	a_0 (1)
			5-DSA/pH 4.0			
5	8.00	1.67	6.95	5.88	33.17	15.33
10	8.00	1.67	7.12	5.89	33.19	15.40
20	7.99	1.70	7.12	5.89	33.05	15.35
40	7.96	1.84	7.21	5.83	33.10	15.38
60	7.93	1.97	7.05	5.89	32.98	15.31
			5-DSA/pH 6.5			
20	7.33	7.83	5.37	5.10	33.03	14.50
40	7.40	6.65	4.98	4.64	33.08	14.23
60	7.32	7.96	5.95	5.16	33.06	14.72
			16-DSA/pH 4.0			
5	8.24	0.97	7.15	6.02	32.36	15.18
10	8.18	1.10	7.09	6.02	32.20	15.10
20	8.14	1.20	7.05	5.98	32.10	15.04
40	8.07	1.40	7.02	5.94	31.98	14.98
60	8.04	1.51	6.98	5.94	31.99	14.97

describe the phenothiazine aggregation. Using EPR spectroscopy, it has been found that the cmc for CPZ changes from 2 mM at pH 5.6 to 0.2 mM at pH 7.3,[47] supporting the increase in aggregation on going from acidic to alkaline medium. On the basis of titration calorimetry studies, values of cmc for CPZ as a function of ionic strength, pH, and temperature were also reported.[48] At 30 °C, it varies from 3.8 to 2.0 mM in the presence of 10 and 500 mM NaCl, respectively. It varies between 7.0 and 2.5 mM for pHs 5.5 and 6.7, respectively.[48] Furthermore, above 20 mM CPZ and at pH 4.0, the EPR spectra for both 5-DSA and 16-DSA are similar to those, characteristic of insertion of the nitroxides in the "micelle-like" aggregates.

In Tables 2 and 3, the EPR parameters obtained from spectral simulations using the NLLS program are shown. First, the magnetic parameters were optimized to obtain an initial rough simulation; then they were fixed and further optimization was performed by varying $\mathbf{R}_{bar}$ as a parameter and maintaining the ratio of $\mathbf{R}_{\parallel}/\mathbf{R}_{\perp} = 10$, also fixed. Finally, the magnetic parameters, and especially the nitrogen hyperfine tensor components, were allowed to change in order to reduce the overall χ^2, improving the final fits, and to obtain some idea on the environment polarity sensed by the nitroxide. A limitation of the NLLS program regarding the information on polarity is the fact that the only way to obtain it is through the hyperfine tensor components. On the basis of this procedure, very good fits were obtained as shown by the symbols in Figures 8 and 9.

Table 2 shows the values of $\mathbf{R}_{bar}$ and τ obtained from the fits for CPZ. Comparison of rotational correlation times shows that at pH 4.0, $\tau = 0.81$ ns for 5-DSA, independent of CPZ concentration in the range 20−60 mM and 0.35−0.49 ns for 16-DSA, increasing with CPZ concentration. So, 5-DSA has a more restricted motion (higher correlation time) as compared to 16-DSA, which would be the expected behavior for nitroxides in micelles. These values are in good correlation with those for surfactant micelles, zwitterionic HPS (0.91 and 0.22 ns) and cationic CTAC (1.03 and 0.20 ns) pure micelles, at pH 4.0, and for the same nitroxides.[49,50] The main difference is that in phenothiazine aggregates the correlation time for 5-DSA is a factor of 2 higher as compared to 16-DSA while for surfactant micelles this factor reaches a higher value of 5.

On going to pH 6.5, a significant motional restriction takes place as indicated by the broadening of the EPR spectra, which is evident for both nitroxides, and by the value of τ for 5-DSA, which is in the range 4.1−3.1 ns (Table 2). However, for 16-DSA (Figure 9) a significant difference occurs in the sense that some broadening and distortion of the spectra remain even at higher CPZ concentrations, suggesting that the spin−spin interaction is not completely removed in this case producing an EPR spectrum of lower intensity. These spectra were not simulated, but estimates of an effective order parameter, *S*, gave values of 0.65 and 0.64, respectively, at 20 and 60 mM (Figure 9, right). These values are somewhat lower as compared to those obtained for 5-DSA of 0.72 and 0.69, respectively, at the same CPZ concentrations (Figure 8, right). Moreover, the maximum hyperfine splittings, A_{max}, were 29.1 and 28.4 G for 5-DSA at 20 and 60 mM, respectively, while for 16-DSA the corresponding estimated values were 28.0 and 27.6 G. Similar to what occurs in surfactant aqueous micelles, the orientational distribution for 5-DSA, as judged from the *S* values, in CPZ aggregates is somewhat more restricted around the normal to the aggregate as compared to 16-DSA.

Previous studies have also shown an increase in motional restriction on going from acid to alkaline medium for nitroxides in the presence of CPZ.[41,47] Stearic acid nitroxides, such as 5-DSA and 16-DSA, undergo a protonation equilibrium with a pK_a close to neutrality, which implies the presence of neutral and anionic species in solution.[51] In the presence of egg yolk lecithin vesicles, the EPR spectrum presents the superposition of two components with slightly different but resolved parameters.[51] The anionic species corresponds to ionized carboxylate in the fatty acid headgroup, producing a higher hyperfine constant, which is consistent with stronger interaction with the lipid headgroup. In ref 41, the association of 5-DSA with CPZ was reported in the presence of lipid liposomes of egg lecithin. Depending on the CPZ concentration in the liposomes, the pK_a for the protonation of 5-DSA was shifted from 7.7 (absence of CPZ) to 4.4 at 0.32 mM of CPZ. According to the authors, this is a general effect for compounds of similar CPZ-like structure since association constants of 100 M^{-1} were observed for both CPZ and the anesthetic dibucaine.[41] It is clear that the formation of this association of 5- DSA or 16-DSA with CPZ would contribute to the increase of motional restriction of the nitroxide, giving higher values of rotational correlation times and effective order parameters. Furthermore, the average nitrogen hyperfine tensor, a_0, is quite similar for both nitroxides at pH 4.0 as well as for 5-DSA at pH 6.5, suggesting that both nitroxides are sensing very similar environments in the phenothiazine aggregates.

In Figures 10 and 11 the EPR spectra observed for TFP aggregates at two pH values, 4.0 and 6.5, and for the two

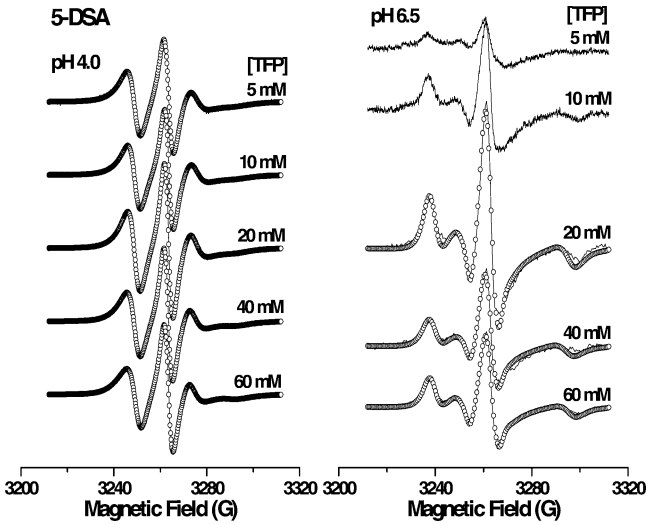

Figure 10. Experimental (full line) and simulated (circles) EPR spectra for 5-DSA bound to TFP aggregates at indicated drug concentrations and pHs.

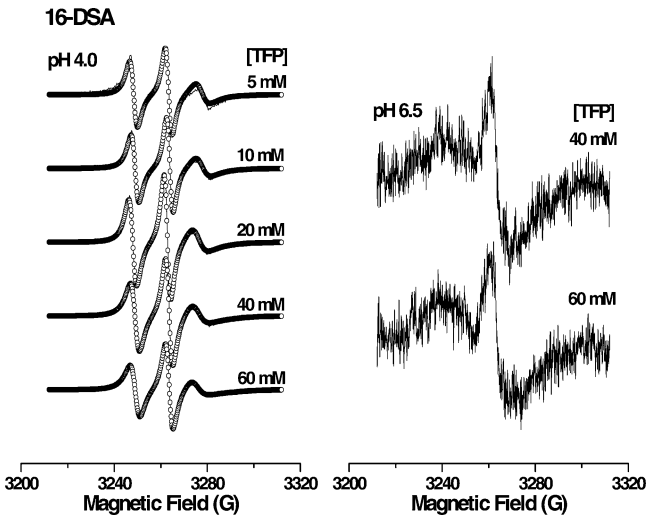

Figure 11. Experimental (full line) and simulated (circles) EPR spectra for 16-DSA bound to TFP aggregates at indicated drug concentrations and pHs.

nitroxides, 5-DSA and 16-DSA, are presented. Similarities and differences are observed as compared to CPZ aggregates. In this case, and differently from CPZ (Figures 8 and 9), at pH 4 the EPR spectra are well resolved in the whole TFP concentration range starting from 5 mM. This means that already at 5 mM of phenothiazine a significant amount of "micelle-like" phenothiazine aggregates is present in solution, and for this reason the broadening due to spin−spin interaction that occurs for CPZ is not observed. This is consistent with a lower cmc value for TFP aggregates as compared to CPZ. The values of the *g*-tensor are very similar as in the case of CPZ. From inspection of EPR spectra (Figures 10 and 11) and Table 3, one can see that the motion of the nitroxides is significantly more restricted as compared to CPZ: the rotational correlation time τ is in the range 1.7−2.0 ns for 5-DSA, and 1.0−1.5 ns for 16-DSA. Here again 16-DSA is somewhat more mobile as compared to 5-DSA, but the differences in τ are smaller as compared to those found both for CPZ aggregates, and especially, for aqueous surfactant micelles. At pH 6.5, in a similar way as observed for CPZ, the EPR spectra could only be simulated for 5-DSA in the TFP concentration range of 20−60 mM. The rotational correlation times obtained from the fits are in the range 6.6−7.9 ns (Table 3), a factor of 2 greater as compared to CPZ aggregates (Table 2), and consistent with strongly immobilized EPR signals. In this case it was not possible to estimate an effective order parameter since the A_{min} spectral feature was not evident. The value of A_{max} was 30.4 G for 20 and 60 mM TFP concentrations, somewhat higher as compared to that for CPZ aggregates and consistent with stronger immobilization of the nitroxide. The average hyperfine constants, a_0, are in the range from 15.0 to 15.4 G for both nitroxides at pH 4.0, with a slightly higher value for 5-DSA. In the case of 5-DSA, at pH 6.5, a_0 was somewhat smaller, around 14.5−14.7 G. For 16-DSA, at pH 6.5, a severe spin−spin interaction took place giving a broad unresolved EPR spectrum, precluding any spectral simulation or semiquantitative estimates. It is interesting that the rotational correlation times for both nitroxides bound to TFP aggregates are a factor of 2 higher as compared to CPZ aggregates, implying either a stronger binding or a more tight packing in TFP "micelle-like" aggregates.

Using the aggregate particle volumes obtained from SAXS data and given in Table 1, the rotational correlation times were estimated for the whole particle from the Debye−Stokes relation, $\tau = \eta V/RT$. They are shown in the last column in Table 1 and can be compared with the values obtained for the nitroxide correlation times in the aggregates, which are presented in Tables 2 and 3 for CPZ and TFP, respectively. It is clear that at pH 4.0, and in a similar way to what occurs with surfactant aqueous micelles,[49,50] the nitroxides undergo a significant additional motion relative to the aggregates since the values of τ are lower as compared to those for the whole aggregate particles. However, the situation is different at pH 6.5, and especially for TFP, where the rotational correlation times obtained for 5-DSA (Table 3) are comparable to the whole aggregate particles values (Table 1). This observation suggests that at pH 6.5 the nitroxides are tightly bound to the aggregates, moving together with the particle as a whole, and having very small residual motion relative to the aggregates. It is also interesting that 16-DSA has a more persistent spin−spin interaction as compared to 5-DSA at both pHs, but especially at pH 6.5. This could be due to the fact that the paramagnetic moiety of 5-DSA is relatively close to its carboxylate group undergoing interaction with the positive charge of the phenothiazine. For 16-DSA the paramagnetic fragment is relatively far away from its carboxylate group. This allows an additional mobility of this group, facilitating the closer approach of such two fragments involved in the spin−spin interactions. Furthermore, the similarity of the a_0 values for both nitroxides could imply a similar location of the probes at the aggregate surface, different from surfactant aqueous micelles or phospholipid bilayer membranes, where 16-DSA senses a more hydrophobic internal environment, and a more clear polarity profile is observed.

4. Conclusions

Phenothiazine molecules studied in the present work are able to self-aggregate in aqueous solutions as a function of both concentration and pH of solution. One of the compounds, chlorpromazine (CPZ), has been extensively studied for more than 30 years focusing the aggregation. The reports found in the literature describe these self-aggregates as "micelle-like" aggregates estimating "critical micellar concentrations" and in some cases giving aggregation numbers. No definitive consensus has been reached regarding the mode of binding of phenothiazine molecules to form the aggregates, either micellar or stepwise. However, the formation of the dimer appears as an

important step in some reports. In the current work, results from a simultaneous SAXS and EPR analysis are reported aiming to further characterize the self-aggregates of CPZ and TFP. These drugs have been previously studied in our laboratory in the context of comicelles formation with a number of ionic surfactants. Our present results have allowed the characterization of the phenothiazine aggregates, although SAXS was only able to provide the aggregate dimensions. Under the assumption of a cylinder model, SAXS parameters were obtained from the fits of scattering data, including the dimensions, anisometry, effective macro-ion charges, and aggregation numbers. Based on the comparison of our low-resolution SAXS results with literature reports on CPZ crystal structure, a model is proposed for the packing of CPZ molecules in the aggregates that correspond to 8−10 unit cells with a vertical stacking along the *c*-direction. EPR data are also quite interesting and suggest that, although at pH 4.0 the aggregates have common features with surfactant aqueous micelles, at higher pH 6.5 significant differences do appear in the dynamics of nitroxide spin labels. One observation is the lack, at this pH, of residual motion of the nitroxide relative to the aggregate since the rotational correlation time for 5-DSA is almost identical to that obtained for the whole aggregated particle from SAXS analysis. An intriguing question remaining for future studies is whether 16-DSA undergoes an intense spin−spin interaction even at the higher phenothiazine concentrations, where the number of aggregates is expected to be high, promoting an effective spin label dilution.

Acknowledgment. Thanks are due to the National Laboratory of Synchrotron Light (LNLS, Campinas, Brazil) for the use of their facilities. This work was supported by research grants from FAPESP and CNPq to R.I. and M.T. A postdoctoral fellowship to W.C. from FAPESP, a Ph.D. fellowship to L.R.S.B. from CAPES, and M.Sc and Ph.D. grants to D.S.N. from FAPESP are appreciated.

References and Notes

(1) Parkànyi, C.; Boniface, C.; Aaron, J. J.; Maafi, M. *Spectrochim. Acta* **1993**, *12*, 1715−1720.
(2) Ford, J. M.; Hait, W. N. *Pharmacol. Rev.* **1990**, *42*, 155−199.
(3) Fowler, G. J. S.; Rees, R. C.; Devonshire, C. *Photochem. Photobiol.* **1990**, *52*, 489−494.
(4) Ramu, A.; Ramu, N. *Cancer Chemother. Pharmacol.* **1992**, *30*, 165−173.
(5) Elisei, F.; Latterini, L.; Aloisi, G. G.; Mazzucato, U.; Viola, G.; Mioio, G.; Vedaldi, D.; Dall'Acqua, F. *Photochem. Photobiol.* **2002**, *75*, 11−21.
(6) Viola, G.; Latterini, L.; Vedaldi, D.; Aloisi, G. G.; Dall'Acqua, F.; Gabellini, N.; Elisei, F.; Barbafina, A. *Chem. Res. Toxicol.* **2003**, *16*, 644−651.
(7) van Iperen, H. P.; van Henegouwen, G. M. J. B. *J. Photochem. Photobiol. B* **1996**, *34*, 217−224.
(8) Wolnicka, A.; Sarna, T.; Knobler, R. *Arch. Dermatol. Res.* **2002**, *294*, 147−151.
(9) Van den Broeke, L. T.; van Henegouwen, G. M. J. B. *Int. J. Radiat. Biol.* **1993**, *63*, 493−500.
(10) Caetano, W.; Gelamo, E. L.; Tabak, M.; Itri, R. *J. Colloid Interface Sci.* **2002**, *248*, 149−157.
(11) Caetano, W.; Barbosa, L. R. S.; Itri, R.; Tabak, M. *J. Colloid Interface Sci.* **2003**, *260*, 414−422.
(12) Barbosa, L. R. S.; Caetano, W.; Homem-de-Melo, P.; Santiago, P. S.; Tabak, M.; Itri, R. *J. Phys. Chem. B* **2006**, *110*, 13086−13093.
(13) Lieber, M. R.; Lange, Y.; Weinstein, R. S.; Steck, T. L. *J. Biol. Chem.* **1984**, *259*, 9225−9234.
(14) Rosso, J.; Zachovski, A.; Devaux, P. F. *Biochim. Biophys. Acta* **1988**, *942*, 271−279.
(15) Luxnat, M.; Galla, H. J. *Biochim. Biophys. Acta* **1986**, *856*, 274−282.
(16) Rodrigues, T.; dos Santos, C. G.; Riposati, A.; Barbosa, L. R. S.; di Mascio, P.; Itri, R.; Baptista, M. S.; Nascimento, O. R.; Nantes, I. *J. Phys. Chem. B* **2006**, *110*, 12257−12265.
(17) McDowell, J. J. H. *Acta Crystallogr., Sect. B: Struct. Crystallogr. Cryst. Chem.* **1969**, *B25*, 2175−2181.
(18) Perez-Villar, V.; Vazquez-Iglesias, M. E.; de Geyer, A. *J. Phys. Chem.*, **1993**, *97*, 5149−5154.
(19) Attwood, D. *Adv. Coll. Interface Sci.* **1995**, *55*, 271−303.
(20) Attwood, D.; Waigh, R.; Blundell, R.; Bloor, D.; Thévand, A.; Boitard, E.; Dubés, J.; Tachoire, H. *Magn. Reson. Chem.* **1994**, *32*, 468−472.
(21) Atherton, A. D.; Barry, B. W. *J. Colloid Interface Sci.* **1985**, *106*, 479−489.
(22) Florence, A. T.; Parfitt, R. T. *J. Phys. Chem.* **1971**, *75*, 3554−3560.
(23) Caetano, W.; Tabak, M. *Spectrochim. Acta* **1999**, *55A*, 2513−2528.
(24) Caetano, W.; Tabak, M. *J. Colloid Interface Sci.* **2000**, *225*, 69−81.
(25) Guinier, A.; Fournet, G. *Small Angle Scattering of X-rays*; Wiley: New York, 1955.
(26) Kotlarchyck, M.; Chen, S. H. *J. Chem. Phys.* **1983**, *79*, 2461−2469.
(27) Glatter, O. *Acta Phys. Aust.* **1977**, *47*, 83−102.
(28) Svergun, D. I.; Feigin, L. A.; Taylor, G. W. *Structure analysis by small-angle x-ray and neutron scattering*; Plenum Press: New York, 1987.
(29) Glatter, O.; Kratky, O. *Small Angle X-ray Scattering*; Academic Press: London, 1982.
(30) Hayter, J. B.; Penfold, J. *Mol. Phys.* **1981**, *42*, 109−118.
(31) Hansen, J. P.; Hayter, J. B. *Mol. Phys.* **1982**, *46*, 651−663.
(32) Chen, S. H.; Sheu, E. Y. In *Micellar Solutions and Microemulsions*; Springer-Verlag: New York, 1990; pp 3−27.
(33) Subczynski, W. K.; Markowska, E.; Gruszecki, W. I.; Sielewiesiuk, J. *Biochim. Biophys. Acta* **1992**, *1105*, 97−108.
(34) Yushmanov, V. E.; Imasato, H.; Perussi, J. R.; Tabak, M. *J. Magn. Reson. B* **1995**, *106*, 236−244.
(35) Alonso, A.; Meirelles, N. C.; Tabak, M. *Biochim. Biophys. Acta* **1995**, *1237*, 6−15.
(36) Berliner, L. J. *Spin labeling: theory and applications*; Academic Press: New York, 1976.
(37) Likhtenshtein, G. I. *Spin labeling in molecular biology*; Wiley-Interscience: New York, 1976.
(38) Schneider, D. J.; Freed, J. H. *Biological Magnetic Resonance*; Plenum Press,: New York, 1989; pp 1−76.
(39) Budil, D. E.; Lee, S.; Saxena, S.; Freed, J. H. *J. Magn. Reson. A 120*, 155−189.
(40) Gelamo, E. L.; Itri, R.; Alonso, A.; da Silva, J. V.; Tabak, M. *J. Colloid Interface Sci.* **2004**, *277*, 471−482.
(41) Louro, S. W. R.; Anteneodo, C.; Wajnberg, E. *Biophys. Chem.* **1998**, *74*, 35−43.
(42) Klein, C. L.; Conrad, J. M., III. *Acta Crystallogr., Sect. C: Cryst. Struct. Commun.* **1986**, *C42*, 1083−1085.
(43) Tehrani, S.; Brandstater, N.; Saito, Y. D.; Dea, P. *Biophys. Chem.* **2001**, *94*, 87−96.
(44) Funasaki, N.; Hada, S.; Paiement, J. *J. Phys. Chem.* **1991**, *95*, 4131−4135.
(45) Attwood, D.; Natarajan, R. *J. Pharm. Pharmacol.* **1983**, *53*, 317−319.
(46) Nichol, L. W.; Owen, E. A.; Winzor, D. J. *J. Phys. Chem.* **1982**, *86*, 5015−5018.
(47) Wajnberg, E.; Tabak, M.; Nussenzveig, P. A.; Lopes, Louro, C. M. B.; S. R. W. *Biochim. Biophys. Acta* **1988**, *944*, 185−190.
(48) Saito, Y. D.; Tehrani, S.; Okamoto, M. M.; Chang, H. H.; Dea, P. *Langmuir* **2000**, *16*, 6391−6395.
(49) Gandini, S. C. M.; Itri, R.; Neto, D. S.; Tabak, M. *J. Phys. Chem. B* **2005**, *109*, 22264−22272.
(50) Santiago, P. S.; Neto, D. S.; Barbosa, L. R. S.; Itri, R.; Tabak, M. *J. Coll. Interface Sci.* **2007**, *316*, 730−740.
(51) Egret-Charlier, M.; Sanson, A.; Ptak, M. *FEBS Lett.* **1978**, *89*, 313−316.